Thermal Study of a Module for SWGO
Southern Hemisphere Wide field-of-view Gamma-ray Observatory

Ricardo Manuel dos Santos Lordelo
ricardo.lordelo@tecnico.pt

Instituto Superior Técnico, Universidade de Lisboa, Portugal

November 2019

Abstract

Under SWGO (Southern Wide Field-of-view Gamma-ray Observatory) Project, this Thesis, developed a numerical analysis tool to simulate the thermal behaviour of a Module for the detection of Gamma radiation. This Module includes a Water Cherenkov Detector (WDC), which comprises a radiation sensor immersed in a water reservoir, and possibly an additional Resistive Plate Chamber (RPC). The Module is to be installed in Andes mountains, Southern Hemisphere exposed to the weather where winter temperatures reach $-10°C$. The Module exchanges heat with its surroundings through its external surfaces. The temperature evolution in critical areas of the Module, e.g. water domain, where freezing may occur, which is detrimental to the acquired data, is studied throughout the yearly climatic cycle. Therefore, the implemented source code uses the Finite Volume Method written in the programming language Python. The created tool uses the Module's characteristics like dimensions, materials, surface properties, etc., and the chosen options like analysis type, initial conditions, geographical location, etc., and the meteorological data (representative of the region) which contains irradiation, air temperature, wind velocity, etc., to calculate the temperature solution at each time step. Results obtained, for the proposed Module, with extreme climate data and the viable mesh refinement, show that the water does not reach $0°C$. Nevertheless, the created tool allows the computation of results with any desired characteristics.

Keywords: Detection Module, Water temperature, Irradiation, Climate Data, Finite Volume Method

1. Introduction

SWGO is an ongoing Project for the installation of a new observatory for Gamma radiation in the Southern Hemisphere. The detection of Gamma radiation uses a Modular detection unit and several detection units placed in a field for flexibility of the observatory layout. A representation of the Module is shown in Figure 1

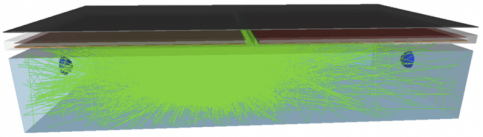

Figure 1: SWGO Module.

The detection of Gamma radiation for this Project uses a Modular detection unit and several detection units placed in a field at altitude, $5000\,[m]$. Figure 2 shows a proposition for the layout of the field.

The Gamma-ray detection Module being studied is comprised primarily of a water reservoir.

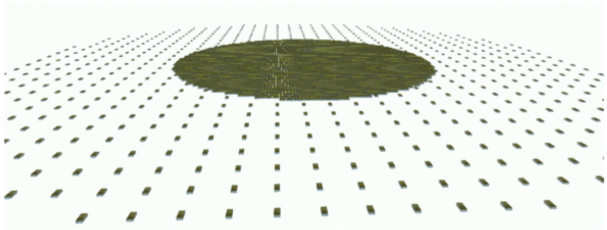

Figure 2: SWGO Array of Modules.

Immersed in the water is the sensor that detects Gamma radiation through the consequences of its existence in the water. This detector is referred to as Water Cherenkov Detector (WCD). Additionally there may be another type of detector placed on top of this water reservoir. This detector is referred to as Resistive Plate Chamber (RPC). It has the same horizontal dimensions. Since the existence of this detector is not yet assured, both scenarios are considered.

2. Background

The Module, exposed to the atmospheric conditions is subject to heat exchange with its surroundings through Conduction, Convection and Radiation [3].

2.1. Convection

The starting point for the governing equations for transient heat transfer and fluid flow is the diffusion equation,

$$\frac{\delta \phi}{\delta t} = \alpha \, \nabla^2 \, \phi \tag{1}$$

If advection is to be added this equation becomes,

$$\frac{\delta \phi}{\delta t} = \alpha \, \nabla^2 \, \phi - \vec{v} \cdot \nabla \, \phi \tag{2}$$

Regarding fluid flow, equating the advection term, second term on the right, to zero yields the continuity equation,

$$\frac{\partial u}{\partial x} + \frac{\partial v}{\partial y} = 0 \tag{3}$$

In a two dimensional case, applying the advection diffusion equation to the velocity components u and v, yields,

$$\frac{\delta u}{\delta t} = \alpha \left(\frac{\partial^2 u}{\partial x^2} + \frac{\partial^2 u}{\partial y^2} \right) - \left(u \, \frac{\partial u}{\partial x} + v \, \frac{\partial u}{\partial y} \right) + X \tag{4}$$

$$\frac{\delta v}{\delta t} = \alpha \left(\frac{\partial^2 v}{\partial x^2} + \frac{\partial^2 v}{\partial y^2} \right) - \left(u \, \frac{\partial v}{\partial x} + v \, \frac{\partial v}{\partial y} \right) + Y \tag{5}$$

Where X and Y represent the body forces, whether sources or sinks.

Applying the advection diffusion equation to the property temperature, yields,

$$\frac{\delta T}{\delta t} = \alpha \left(\frac{\partial^2 T}{\partial x^2} + \frac{\partial^2 T}{\partial y^2} \right) - \left(u \, \frac{\partial T}{\partial x} + v \, \frac{\partial T}{\partial y} \right) + S_T \tag{6}$$

The sources of heat through dissipation of viscous shear stresses are disregarded here since their effect is small in this study.

These are the governing equations for the convection process.

In natural convection the main source of momentum in the fluid is its buoyancy due to density difference due to temperature difference. This body force is responsible for momentum creation and may be approximated with the difference in density from each fluid element to the average density which may be a function of temperature, equation 7.

$$(\rho - \rho_\infty) \, g_i = -\rho_0 \, g_i \, \beta \, (T - T_\infty) \tag{7}$$

This is called the Boussinesq approximation.

If there is an imposed upstream velocity u_∞ and its magnitude is higher than the velocity related to buoyancy effects, convection is referred to as forced in contrast to natural convection. In the mean term there is what is referred to as mixed convection where both velocities are similar in magnitude.

The flow characteristics are obtained through dimensionless groups. These quantities are drawn from the equations governing the flow stated above after simplifications relative to each specific situation (forced / free) and normalizing their terms. Each dimensionless group has its own meaning and inform about a specific characteristic. A detailed view of this subject in present in [3, 4].

Symbol	Group	Definition
Nu_L	Nuselt number	$\frac{hL}{k_{fluido}}$
Pr	Prandtl number	$\frac{c_p \mu}{k} = \frac{\nu}{\alpha}$
Re_L	Reynolds number	$\frac{U \cdot L}{\nu}$
Gr_L	Grashof number	$\frac{g\beta(T_s - T_\infty)L^3}{\nu^2}$
Ra_L	Rayleigh number	$Gr_L \cdot Pr$

Table 1: Dimensionless groups for heat transfer.

2.2. Radiation

The Sun is the main source of heat in the Module. Direct solar radiation arrives at the Earth surface without being absorbed or scattered by the atmosphere, diffuse solar radiation accounts for the part of the radiation that arrives at the earth surface after interfering with the atmosphere without being absorbed. These are stated in the climate data file. There is also radiative heat exchange between the Module and the atmosphere which is obtained through approximating of the atmosphere to a black body and considering a two surface enclosure which yields equation 8

$$q'' = \varepsilon_1 \, \sigma \, (T_{sky}^4 - T_{obj}^4) \tag{8}$$

3. Implementation

The subject of how the temperature profile in the Module during one year is addressed here. The details of the computational implementation are explained, namely, the choices made and why for each option of the implementation. Even though the basics of the method is well defined, several option regarding the approximation schemes need to be considered individually and decided upon according to

this particular case.

3.1. Finite Volume Method

FVM is a method for solving partial differential equations (PDE). In this method, the solution of some property is calculated at discrete Volumes in a meshed geometry. In this method, the volume integral of the PDE's are converted to surface integrals using the Gauss's divergence theorem [6, 7].

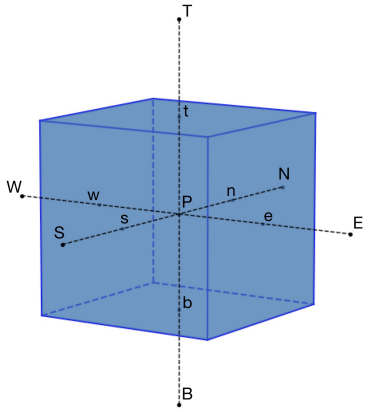

Figure 3: Control Volume.

FVM implements the conservation laws of a scalar intensive property ϕ all round a Control Volume (CV). This CV has constant properties within itself and the rate of change of property ϕ, happens through its faces whether by advection or diffusion.

Integrating the advection-diffusion equation over the entire CV, yields the conservation of a property about the CV's volume or within the boundaries of the CV.

$$\begin{aligned} &\int_V \frac{\partial(\rho\,\phi)}{\partial t}\,dV + \int_V div\,(\rho\,\phi\,\vec{v})\,dV = \\ &= \int_V div\,(\Gamma\;grad\,\phi)\,dV + \int_V S_\phi\,dV \end{aligned} \tag{9}$$

Then applying the Gauss Divergence theorem, the same information is provided, but now, what happens within the CV's is related to what happens at its surfaces.

$$\begin{aligned} &\frac{\partial}{\partial t}\left(\int_V \rho\,\phi\,dV\right) + \int_A \vec{n}\,(\rho\,\phi\,\vec{v})\,dA = \\ &= \int_A \vec{n}\,(\Gamma\;grad\,\phi)\,dA + \int_V S_\phi\,dV \end{aligned} \tag{10}$$

After some algebra, the transient advection diffusion equation applied to a finite volume discretisation domain, a CV, for a property ϕ at each time step yields equation 11.

$$\begin{aligned} &\frac{\rho\,(\phi_{CV}^{t+\Delta t} - \phi_{CV}^{t})}{\Delta t}\Delta x = \phi_W\,(C_w + D_w) - \\ &-\phi_{CV}\,(-C_w + C_e + D_w + D_e) + \\ &+\phi_E(-C_e + D_e) \end{aligned} \tag{11}$$

This equation is used for implementing the governing equations of fluid flow and heat transfer presented in the next Table 2.

Gov. Equation
$\frac{\partial\rho}{\partial t} + div\,(\rho\,\vec{v}) = 0$
$\frac{\partial(\rho\,u)}{\partial t} + div\,(\rho\,u\,\vec{v}) = div\,(\mu\;grad\,u) + S_{Mx}$
$\frac{\partial(\rho\,v)}{\partial t} + div\,(\rho\,v\,\vec{v}) = div\,(\mu\;grad\,v) + S_{My}$
$\frac{\partial(\rho\,w)}{\partial t} + div\,(\rho\,w\,\vec{v}) = div\,(\mu\;grad\,w) + S_{Mz}$
$\frac{\partial(\rho\,T)}{\partial t} + div\,(\rho\,T\,\vec{v}) = div\;(^{k}/_{c_p}\;grad\,T) + S_T$

Table 2: Governing Equations for fluid flow with heat transfer.

3.2. Numerical Approach

A fully implicit scheme is used for the change of ϕ over time. This scheme uses the values of ϕ at $t+\Delta t$ which are unknown.

The scheme used for approximating the fluxes of ϕ at the CV faces is the Hybrid scheme for its robustness and stability. Succinctly, this scheme disregards the influence of diffusion when it is small enough, which is translated by the *Peclet* number, equation 12.

$$Pe = \frac{\rho\,u}{\Gamma/\delta\,x} \tag{12}$$

Another method adopted was the staggered grid for the velocity field which makes for a more robust and stable calculation especially in the case of coarse grids. This method avoids the interpolation of the pressure field by implementing the velocities at the CV faces, therefore, the pressure gradient at the staggered velocity CV has its face values coincident with the two adjoining CV values of the pressure field grid. Hence no interpolation is needed. The staggered grid has to be implemented in all three directions.

The geometry in this implementation is comprised of several blocks, each block with a single material, whether solid or liquid, and with a well defined position relative to the other blocks. Each block may have an independent mesh refinement. Each one of these blocks as an extra layer of CV's all around the block that provide the means to store the boundary conditions relative to this block. Once all blocks are built, an assembly phase takes place. Each block is connected to its adjoining blocks using the extra CV's. This connection must be fully conservative for the properties under analysis. If the block belongs to the periphery, of the

Module, one of its faces is has the Module's boundary conditions.

If block 1 has three CV's that need to be connected to one CV of block 2, the temperatures of CV4, CV5 and CV6 are set equal to the temperature of CV8, and the temperature of CV7 is set equal to the average of the temperatures of CV1 , CV2 and CV3 . The connection between these blocks is shown in Figure 4.

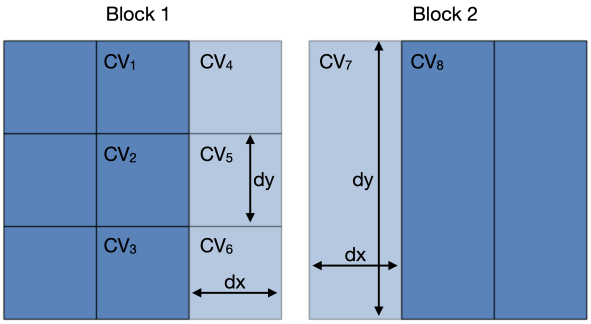

Figure 4: Connection between Blocks.

3.3. Geometry

The dimensions of the Module are fixed throughout this Thesis, but may be changed if desired since they are an input parameter.

The water volume has an horizontal surface area of $1 \times 1\ [m]$ and a height of $0.5\ [m]$. A $1\ [m]$ sided cube is also considered. The rest of the geometry (parts of the Module) are added to these base dimensions of the water itself.

Figure 5 shows the Module with all its possible constituents, RPC and insulation. The water is contained by a reservoir. Inside this reservoir there is an air gap between the water surface and the upper surface of the reservoir. Above the upper part of the reservoir, there is another air gap, then the RPC, then another air gap, a lead plate and finally an insulation layer.

In its simplest form, there is only the water, the air gap above it and the reservoir without the upper protrusion to hold the RPC and lead plate. Dimension wise, and adding to the water volume, the thickness of the walls of the reservoir itself is $1.5\ [cm]$ and the thickness of the insulation is $4\ [cm]$. These values are rough estimations of the foreseeable ones since these are not defined yet. The height of the air gaps is assumed to be $5\ [cm]$. The thickness of the Lead Plate is $5.6\ [mm]$ and the overall thickness of the RPC is $2.8\ [cm]$. Figure 6 shows a closeup of the upper constituents of the Module, corresponding to the area marked with a dashed line in Figure 5.

The RPC, is implemented as several layers

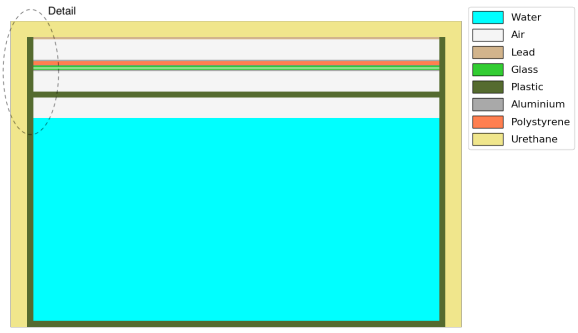

Figure 5: Module Geometry with RPC and insulation.

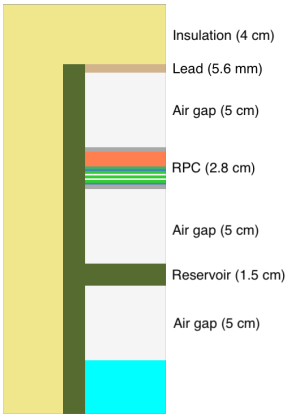

Figure 6: Detail of Lead Plate, RPC and Water.

stacked on top of each other. Each layer represents each of the main constituents of the RPC. The actual RPC, is made of several more minor parts like spacers and sidewalls that are not taken into account here.

One, two and three-dimensional geometries are shown in the next Figures 7, 8 and 9. The dimensions in Figures 8 and 9 are not proportional to the real ones for clarity sake. Here, the water, instead of having a $1\ [m]$ side, has $10\ [cm]$ and the other dimensions relative to the water are kept the same. Figure 5 shows the Module with its real proportions.

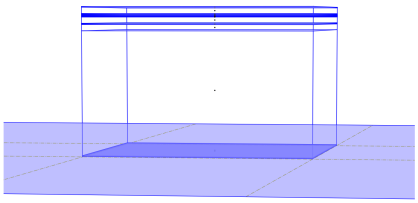

Figure 7: Module with RPC.

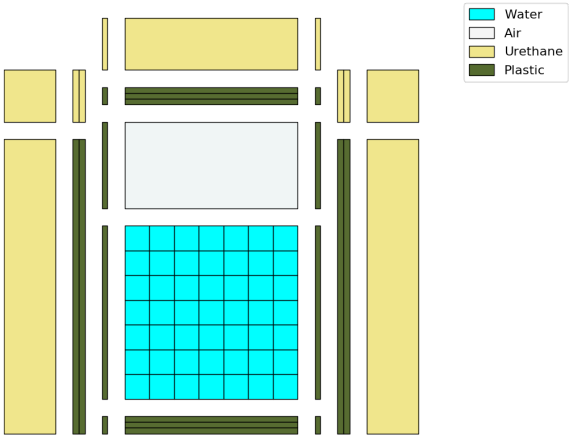

Figure 8: Bidimensional Grid without RPC and with Isolation.

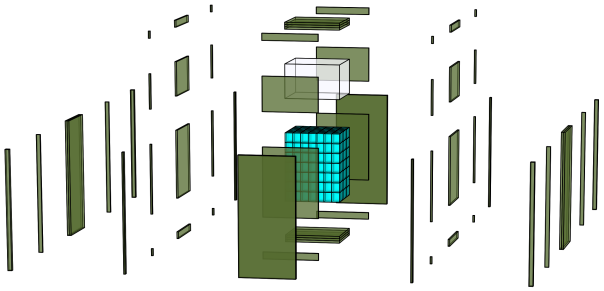

Figure 9: Tridimensional Grid.

The geometry domain shown above is not the complete geometry but only the part of the Module. In the actual domain under calculation, there is an underground part that is not represented in these drawings. This part makes an adiabatic condition at the bottom of the geometry possible. The lateral sides of the domain underground are also adiabatic. This part of the domain extends to a depth where temperature variation throughout the year is considered approximately zero, $10\,[m]$. This depth is conservative according to the analytical solution for conditions that roughly approximate the Module situation. The solution is for a semi infinite solid with constant surface temperature [1], equation 13.

$$\frac{T(x,t) - T_s}{T_i - T_s} = erf\left(\frac{x}{2\sqrt{\alpha\, t}}\right) \tag{13}$$

$10\,[m]$ is approximately the depth at which there is no temperature difference after a 6 months period for constant surface temperature, a dimensionless temperature at $T^*(x\,,\,t) = 0.999$ and initial temperature of the semi infinite solid.

The grid in this block has a distinct treatment with an increasing height of the next CV's in the depth direction, meaning the deepest CV has the highest volume. Figure 10 shows the one-dimensional case with the underground discretization.

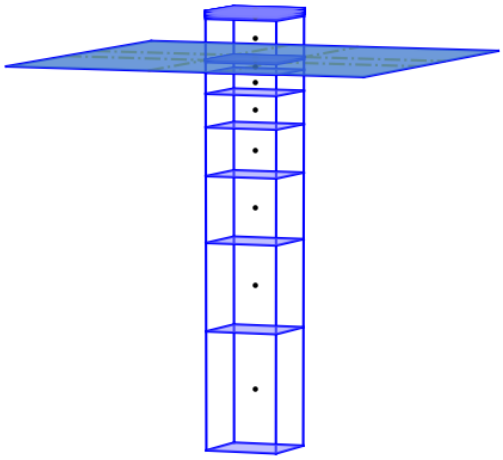

Figure 10: Unidimensional Geometry.

Two-dimensional analysis may be used to approximate a situation where the Modules are stacked together in a row and consequently there is some symmetry in this direction.

Three-dimensional case, although the most reliable, has a high computational cost relative to the used computer in this Thesis (Processor - 2,3 GHz Intel Core i7, Memory - 4 GB 1600 MHz DDR3).

3.4. Boundary Conditions

For the one-dimensional case the boundary conditions apply at the top and the bottom of the geometry. For the two-dimensional and three-dimensional case, the lateral boundary conditions are added.

The underground, or subterranean part has an adiabatic condition at the walls and bottom surfaces. The lateral walls above ground and the upper surface of the Module, are subject to the climatic conditions hence exchange heat with its surroundings through convection and radiation.

The correlations used for the surfaces of the Module are distinct for the top horizontal surface and lateral surfaces. In each of these surfaces, convection may be free, forced or mixed. In each of these cases there may be a laminar or a turbulent flow which impose different correlations. All these characteristics are dictated through the dimensionless parameter shown in Table 1.

In the inside of the Module there is convective heat transfer in the air and water enclosures. These are also correlated for the air and water, although, for the water, a numerically obtained convective flow was implemented which may or may not be used.

If correlations are applied to the water, restrictions in their range of applicability make for an approximation to the heat transfer that is not realistic in some cases. For example in the one-dimensional case the enclosure correlation used is perfectly suited because the lateral walls are considered adiabatic, but in the more realistic three-dimensional case the lateral walls are not adiabatic and the best approximation would be a case where heat transfer through these lateral walls is small when compared to the vertical direction.

Regarding radiative heat exchange, its direct and diffusive components are included in the climate data file. The angle between the direct solar radiation and the normal to any surface in any geographical position at any time and date during day time is given by equation 14, [2].

$$\begin{aligned} cos\,\theta \quad = \quad & sen\,\delta\ sen\,\phi\ cos\,\beta \\ & -sen\,\delta\ cos\,\phi\ sen\,\beta\ cos\,\gamma \\ & +cos\,\delta\ cos\,\phi\ cos\,\beta\ cos\,\omega \\ & +cos\,\delta\ sen\,\phi\ sen\,\beta\ cos\,\gamma\ cos\,\omega \\ & +cos\,\delta\ sen\,\beta\ sen\,\gamma\ sen\,\omega \end{aligned} \tag{14}$$

ϕ represents Latitude, δ declination of the Sun at solar noon, *beta* is the inclination relative to the horizontal, γ is cardinal orientation of the surface in question, ω the solar hour angle, 15° per hour and finally θ the aforementioned angle between the normal to the surface and the $Zenith$ angle θ_z [2].

Then in order to compute the total irradiance at a surface, a model by Liu and Jordan (1963) [2], is used,

$$\begin{aligned} G_T = G_{dir}\left(\frac{cos\,\theta}{cos\,\theta_z}\right) + G_{dif}\left(\frac{1+cos\,\beta}{2}\right) \\ +(G_{dir}+G_{dif})\rho\left(\frac{1-cos\,\beta}{2}\right) \end{aligned} \tag{15}$$

Where $\frac{(1+cos\,\beta)}{2}$ and $\frac{1-cos\,\beta}{2}$ are the view factors of the sky to the surface and the ground to the surface respectively, ρ is the reflectance of the ground, which in this study is assumed to be $\rho = 0.4$, sand reflectance [3].

Lastly the sky radiation is obtained with the use of equation 8 and T_{sky}. Again a correlation is used given by Swinbank (1963) [2], which relates the sky temperature to the air temperature with the simple relation, $T_{sky} = 0.0552\,T_{amb}^4$.

3.5. Convection in Enclosures

When correlations are used for convection, the outcome is a convection coefficient for the fluid geometry. In order to implement the corresponding heat transfer in the FVM, a diffusion coefficient is required which is the thermal conductivity of the material in question. In the case of correlated convection the diffusion coefficient must be translated to an equivalent conductivity coefficient in order to be implemented. This is accomplished by equating the heat flux through a CV using Newton's law of cooling and the Fourier's law. The result is shown for a one-dimensional case in equation 16, where $_{e,w}$ represent east and west faces of the CV.

$$q = A\,h\,\Delta T_{e,w} = A\,k_{eq}\,\frac{\Delta T_{e,w}}{\Delta x_{CV}} \implies k_{eq} = h\,\Delta x_{CV} \tag{16}$$

3.6. Properties and Constants

For the solid materials, constant thermal properties are assumed. If the material is a fluid, these properties may change with temperature. For example the air density is variable according to its temperature. Although all these properties are considered constant within each time step, they are updated at each time step. Nevertheless the differences in doing so are small if the temperature range in question is not great. Hence, for the air and water there is a correction at each time step. The air correlates its density through the ideal gas law, shown in equation 17.

$$\rho = \frac{p}{R_{specific}\,T} \tag{17}$$

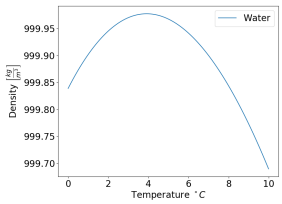

Figure 11: Water Density.

The water has a particular behaviour regarding its density to temperature relation. Density decreases upon cooling below a certain temperature at a certain pressure. For a pressure of $1[atm]$ the

point of zero coefficient of volumetric expantion is about $4°C$. The used data for water density is taken from [5]. This data is represented in Figure 11. Another aspect is that upon freezing, it lowers its density which is contrary to most other materials that contract when going from a liquid phase to a solid phase.

Material	ρ $[kg/m^3]$	k $[W/m \cdot K]$	c_p $[J/kg \cdot K]$	μ $[N \cdot s/m^2]$
Water	Var.	Var.	Var.	Var.
Air	Var.	0.0263	1006	Var.
Sand	1515	0.27	800	n/a
Lead	11340	35.3	129	n/a
Glass	2500	1.4	750	n/a
Plastic	1300	1.4	1465	n/a
Aluminium	2770	177	875	n/a
Polystyrene	16	0.04	1210	n/a
Acrylic	1300	1.4	1465	n/a
PCB / FR4	1850	0.32	396	n/a
Polyurethane	70	0.026	1045	n/a

Table 3: Additional input parameters.

4. Results

The presented results are limited to their availability. The most interesting results are also the most time consuming (three dimensional with convective flow in the water domain). All presented results use a time step of one minute.

The tool developed for the thermal analysis is available for use to obtain solutions with the desired Module's characteristics and available options, e.g. surface properties, general dimensions, type of analysis, RPC, insulation and its thickness, cardinal orientation, geographical location, etc. The used climate data file is provided but a data file with different meteorological scenarios may be used. Section 5 has a link to these files.

The results focus on differentiating factors that may influence the temperature solution. Hence several test cases are compared against each other so that conclusions to the response of this differentiating factors may be drawn.

4.1. Problem Description

The climate data is obtained by interpolation of nearby meteorological stations for air temperature and wind speed at the location of the Observatory and for direct and diffuse solar radiation uses also satellite data . This data is shown in Figure 12.

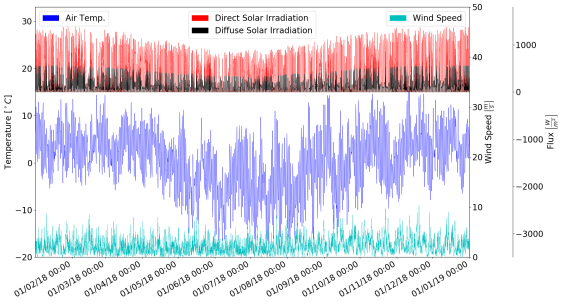

Figure 12: Climate Data Set.

Other input variables are stated in Table 4. The initial temperature is assumed, in this case, to be constant throughout the entire domain, Module and ground, although they may be set distinct from each other in this implementation.

Latitude	Longitude	Initial Temp.
$22° \, 56' \, 53.6'' \, S$	$68° \, 12' \, 43.4'' \, W$	$2 \, [° \, C]$
Absorptance	Emissivity	Reflectivity
0.9	0.4	0.4

Table 4: Additional input parameters.

The different situations considered for analysis are stated in Table 5. When used, the insulation thickness is $5 \, [cm]$. All other dimensions are according to Section 3.

Case	Height of Water	RPC	Isolation
1	$1 \, [m]$		
2	$0.5 \, [m]$		
3	$1 \, [m]$	✓	
4	$0.5 \, [m]$	✓	
5	$1 \, [m]$		✓
6	$0.5 \, [m]$		✓
7	$1 \, [m]$	✓	✓
8	$0.5 \, [m]$	✓	✓

Table 5: One-dimensional test instances.

4.2. One-Dimensional

Figure 13 shows the obtained average temperature of the water during one year for all eight cases.

In case 1 and 2, the temperature does not fall below $\approx 3 \, °C$. This is due to the water thermal expansion coefficient, β, that changes its sign at $\approx 3.9 \, °C$, being negative below this temperature. Hence, if the temperature of the water is below this threshold, convection exists when the temperature of its upper surface is above that of its lower surface,

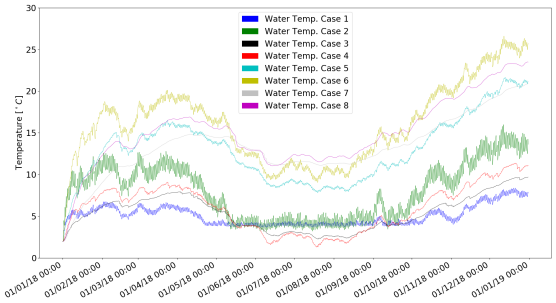

Figure 13: One-dimensional Water Temperature, Cases 1 through 8.

and vice versa. When in convection, the thermal resistance of the water is lower, hence, taking into account that the upper surface assumes most of the temperature variation between both the upper and lower surface of the water and the bottom part is approximately at the same temperature as the water, when the water has a temperature $< 3.9\,°C$ and its upper surface is hotter, the heating heat flux is convective. If the upper surface is cooler, is conductive. If the water is at a temperature $> 3.9\,°C$, the opposite happens, convection upon cooling and conduction upon heating. Therefore, there is a tendency for the temperature of the water to stay $\approx 3.9\,°C$. The sun irradiation (the main heat source in the Module) is sufficient to rise the temperature to this threshold value during day time.

Comparing cases 1 and 3, it can be seen that in case 3, the temperature drops below this threshold value. This is due to the presence of the RPC. The several layers of different materials above the water in case 3 dampen the large temperature range due to the day / night cycle in the upper surface of the water. Consequently, in case 3, the air above the water has a lower temperature range than case 1 because the air cavity has a higher thermal resistance to the surface of the Module.

Case 3 spends most of the time in the winter months (June - August) with an air enclosure temperature below the threshold value of $3.9\,°C$. Hence, although through conduction, the water does not gain heat significantly since the upper surface of the water rarely has a temperature above the lower surface, and does not undergo convection as often as case 1. In contrast, case 1 does nearly every day, which is the cause for maintaining its temperature above $\approx 3\,°C$ during winter.

A close up view of this situation is shown in Figure 14 where the convection coefficient for case 3 is represented through its symmetric for convenience.

As may be seen, cases 1 through 4 have a general lower temperature than cases 5 through 8. This is because of the isolation that, again lowers the temperature range in the air above the water.

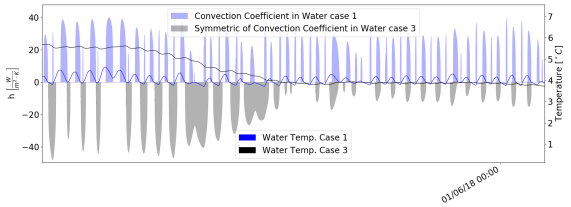

Figure 14: One-dimensional Convection in Water, detail, Cases 1 and 3.

For the RPC, the temperatures of the middle glass plate in cases 3 and 4, are represented in Figure 15 where the first plot is from case 3 and the second is the difference in temperature between them which is minimal.

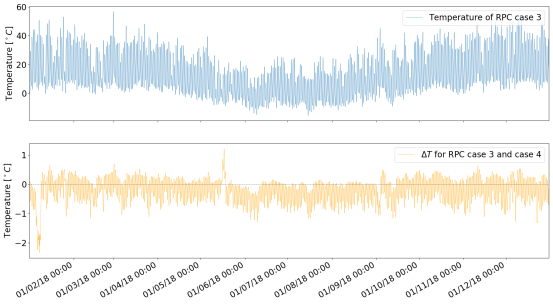

Figure 15: One-dimensional Temperature of RPC, Cases 3 and 4.

4.3. Two-Dimensional

The two-dimensional case may be calculated in two manners regarding convective heat transfer in the water domain. One uses correlations as in the one-dimensional case, the other calculates the convective flow in the water. The latter is computationally heavy hence its results are incomplete to date.

Results with Convection Correlation for case 1 is presented in Figure 16. The temperature does not drop below $4°C$ keeping a positive coefficient of thermal expansion throughout the year.

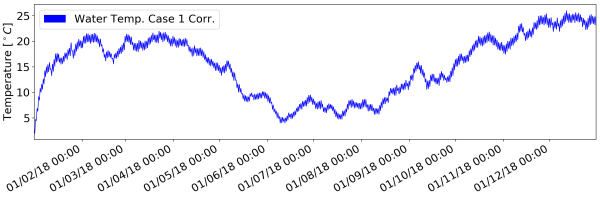

Figure 16: Two-dimensional Water Temperature using convection correlation, Case 1.

The main difference in the two-dimensional case with convective correlation when compared to the one-dimensional case is the temperature fluctuation

within one day is higher. It is so due to the two additional faces exchanging heat with the atmosphere.

Regarding results with Convective Flow, the results for the eight cases used for the one-dimensional results are presented up to the available solution for all the eight cases since the entire year is not yet calculated. Figure 17 shows the results for the water temperature.

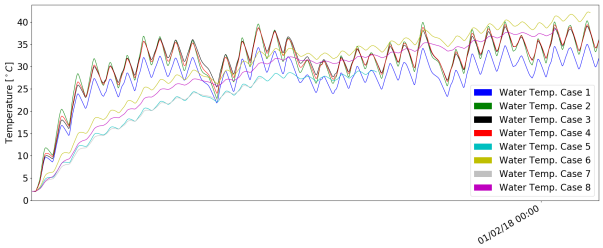

Figure 17: Two-dimensional Water Temperature with convective flow, Case 1 through 8.

The higher temperature of the water is noticeable when compared to the two-dimensional with correlation results. The higher heat exchange with the water in the convective flow analysis lowers the temperature gradients between the water and the walls hence the temperature of the surface of the walls does not fluctuate as much. For instance, during day time, when irradiation is heating the surfaces of the Module, the temperature of the surface is regulated by this higher heat transfer with the water lowering convection heat loss to the exterior due to a decrease in the wall exterior surface temperature.

All cases use a mesh refinement in the water of 8×8 CV's.

4.4. Three-Dimensional

Three dimensional result have limited availability. These are the most interesting results since they use all the implemented material for obtaining a solution.

The available results with Convection Correlation in the Water are shown in Figure 18.

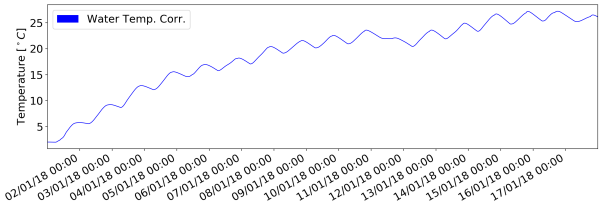

Figure 18: Three-dimensional, correlated convection, water temperature.

The behaviour is similar to the two dimensional case, but the temperatures are higher due to the same reason, two additional walls.

Results with Convective Flow in the Water have the least availability. The first day is computed thus far. This incomplete solution is shown in Figure 19.

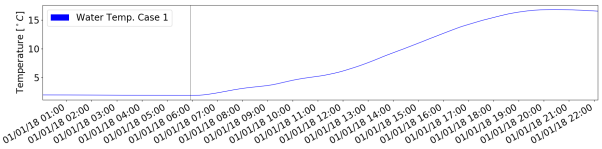

Figure 19: Three-dimensional, water temperature.

The water temperature, reaches $\approx 15°C$ in the first day, due to the additional faces. This behaviour is also present in the cooling phase during night time. Figure 20 shows a close up of the water temperature during night time. The vertical line in both Figures represents sun rise.

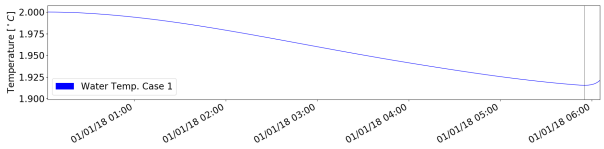

Figure 20: Three-dimensional, water temperature, cooling.

Besides the additional lateral walls, many factors influence this temperature evolution, for example, convection is different in the three-dimensional case, the sun's irradiation is slightly higher because of the declination of the sun, etc.. Hence the entire yearly solution wold have to be obtained in order to draw conclusions regarding temperatures in the water.

5. Conclusions

Conclusions regarding the actual water temperature should be based at least in the two-dimensional if not in the three-dimensional case.

For the one dimensional case the increase in insulation to the water whether from the RPC or from the $5[cm]$ of insulation material or both, results in a general temperature increase in the water throughout the year. The decrease of this insulation on top of the water will on the other hand increase, not its general temperature, but rather its minimum temperature, since the increase of temperature in the water is faster than its decrease below $\approx 3.9°C$ hence, at this temperature, the temporary high solar radiation during day time provides a sufficient increase to the water temperature in order to compensate for the losses during night time if insulation is present.

The two dimensional case using convection correlation in the water shows a similar behaviour but with a higher daily temperature range in the water due to the two additional faces exposed to the atmospheric conditions. The two-dimensional case with convective flow in the water shows a higher temperature of the water in general. This is due to a higher heat transfer between the water and the side walls. In other words, the heat gain from the sun in a side wall is relatively more absorbed by the water in comparison to the correlated case where heat transfer to the water is through conduction in the side walls.

The three dimensional results present a too short time period to draw meaningful conclusions. Nevertheless the maximum temperature reached in the first day is the highest of all results. Hence it foresees a higher daily temperature range and also, although less predictable, yearly temperature range. The shown behaviour so far is similar to the two dimensional qualitatively.

The main concern motivating the proposition of this Thesis, is the freezing of the water in the reservoir. Based on the gathered results there is no tendency for the water temperature to drop to $0\,^{\circ}C$. This scenario is, of course, based on the used input and type of analysis, and must be interpreted accordingly. For example, if a colder climate data set were to be used, naturally the water temperature would be lower as well. Or if the surface is not painted black, that is assumed in all cases, the radiative heat gains would be lower, hence the water temperature be lower.

The differentiating factors that were compared in Section 4 show a more or less predictable result. As long as the climacteric conditions are known and the domain is well defined regarding properties of materials, boundary conditions etc., the qualitative aspects of the results are foreseeable with regard to the influence of each differentiating factor. Nevertheless, since, for example, freezing of water happens at a discrete temperature, calculation of the temperatures in the Module is always necessary.

One of the main achievements of this Thesis is the tool developed for temperature analysis. A brief description of this application is available in the Thesis itself. It may be downloaded through the following link:

https://drive.google.com/drive/folders/1IUb98jXzMq2qHkeqdw3LTl6SKiuMZbvK?usp=sharing where an application to be run in Mac OS plus a freely available climate data file are available. Through this application, the most important input variables may be defined and set in the pre processor phase, and the results may be clearly viewed.

Acknowledgements

I would like to thank both my Supervisors, Prof. Pedro Jorge Martins Coelho and Prof. Luís Filipe Moreira Mendes.

References

[1] H. Carslaw and J. C. Jaeger. *Conduction of Heat in Solids*. Oxford University Press, second edition edition, 1959.

[2] J. A. Duffie and W. A. Beckman. *Solar Engineering of Thermal Processes*. John Wiley & Sons, 1980. ISBN:0-471-05066-0.

[3] F. P. Incropera and D. P. Dewitt. *Fundamentals of Heat and Mass Tranfer*. John Wiley & Sons, fith edition edition, 2002. ISBN:0-471-38650-2.

[4] S. Kakaç, R. K. Shah, and W. Aung. *Handbook of Single-Phase Convective Heat Transfer*. John Wiley & Sons, 1987. ISBN:0-471-81702-3.

[5] D. R. Lide. *CRC Handbook of Chemistry and Physics*. CRC Press, 74th edition, 1993 - 1994.

[6] M. Peric and J. H. Ferziger. *Computational Methods for Fluid Dynamics*. Springer, 3rd edition edition, 2002.

[7] H. K. Versteeg and W. Malalasekera. *An Introduction to Computational Fluid Dynamics*. Pearson Education Limited, second edition edition, 2007.